



An Amalgam of Mg-Doped TiO₂ Nanoparticles Prepared by Sol–Gel Method for Effective Antimicrobial and Photocatalytic Activity

N. Nithya¹ · S. Gopi² · G. Bhoopathi³

Received: 21 May 2021 / Accepted: 18 July 2021 / Published online: 15 September 2021

© The Author(s), under exclusive licence to Springer Science+Business Media, LLC, part of Springer Nature 2021

Abstract

In this study, undoped and Magnesium doped TiO₂ nanoparticles (Mg-TiO₂ NPs) are successfully synthesized via a simple sol–gel method cost-effectively. The prepared Mg- TiO₂ NPs is characterized by UV–Vis, FTIR, PL, XRD, FESEM, TEM, and EDAX. UV–Visible Spectroscopy showed that an increase in the optical bandgap concerning the concentration of dopant Mg increases. The bandgap values were found to be 3.57–3.54 eV. FTIR spectra shows that the presence of the characteristic stretching and bending vibrational band of Ti–O bonding at 468 cm^{−1} and shifts in vibrational bands were observed for Mg-TiO₂ NPs. PL spectra of Mg- TiO₂ NPs at different concentrations exhibit a strong UV emission band. X-ray diffraction confirmed the formation of the tetragonal anatase phase. The average crystallite size of synthesized samples was found to be 22–19 nm. The average crystallite size of Mg- TiO₂ NPs decreases with increasing the concentration of dopant Mg. The FESEM and TEM analysis confirmed that the spherical morphology for both TiO₂ and Mg-TiO₂ NPs. SAED pattern confirms the crystalline nature of prepared samples. EDAX spectra confirm the presence of Ti, O, and Mg and confirm that Mg²⁺ ions are present in the TiO₂ lattices. The prepared samples were investigated against gram-positive and gram-negative bacteria. The prepared samples exhibit potent antibacterial activity against gram-negative bacteria than the gram-positive bacteria. The prepared samples exhibit significant photocatalytic degradation for Methylene blue (MB).

Keywords Mg-TiO₂ NPs · Structural properties · Reactive oxygen species · Antibacterial activity · Photocatalytic activity

1 Introduction

Nanotechnology has a wide range of applications such as electronics, catalysis, agriculture, optical communications, food packaging, etc. [1–3]. In the present era, nanomaterials have a greater interest in many fields because of change their optical and physical properties when particle size reduces to the nanoscale. The recent studies on semiconductor nanoparticles also suggested that optical bandgap becomes increased that as particle size decreased thereby change in its optical and electrical properties and thus making the nanomaterials suitable for several applications [4–6]. The performance

of nanomaterials depending on the size and shape that are affected by the high surface to volume ratio. Different types of nanomaterials are used to enhance the optical, electrical, thermal, photocatalytic, antibacterial, and gas sensing properties [7, 8]. Exploiting solar energy for elimination of the variant kinds of organic contaminants from water with the help of photocatalyst has been offered as a logical and advantageous path to obviate the topic of energy trouble. Solar energy can be transformed to chemical energy with application of photocatalyst [9–11]. Fe₂O₃, WO₃, Bi₂O₃, MgO, ZnO, and TiO₂ are the most semiconductor nanomaterials that are used for photocatalyst, antibacterial applications, and safe for human beings, animals, and plants [12]. Among all the metal oxide nanomaterials, TiO₂ is an n-type semiconductor with a wide bandgap of 3.2 eV, UV light absorption, high chemical and thermal stability, and tetragonal structure [13]. TiO₂ has many applications in the field of biomedical, photocatalytic activity, antibacterial activity, gas sensors, solar cells, agriculture, water purification, textiles, food packaging, etc. [14].

✉ N. Nithya
nithyanesakumar@gmail.com

¹ Department of Physics, PSGR Krishnammal College for Women, Coimbatore 641004, India

² Department of Physics, SRMV College of Arts and Science, Coimbatore 641020, India

³ Department of Physics, PSG College of Arts and Science, Coimbatore 641014, India

Chemical and physical attribute and efficiency of the nanoscale compounds can be dependent to fabrication path, size distribution, purity rate, shape of them [15]. To date, intense research attempt has been undertaken to adjust size distribution, purity rate, shape of the nanoscale compounds [16].

TiO_2 occurs in three crystalline forms such as anatase, rutile, and brookite phase. These three forms have high refractive index values, which are 2.488, 2.609, and 2.583 respectively. Among these three forms, anatase is metastable, rutile is highly stable and brookite is unstable [17].

The anatase form is considered the most physically and chemically active phase of TiO_2 [18]. Shape and size-controlled synthesis of TiO_2 nanoparticles enhance its properties have been extensively studied in recent years [19]. There are several methods for the synthesis of TiO_2 nanoparticles such as sol-gel [20], wet chemical [21] co-precipitation [22] hydrothermal [23] ball milling [24] combustion [25], and biological method [26]. Among these methods, sol-gel is the most feasible method for the synthesis of TiO_2 nanoparticles because of its ability to control size and surface morphology. The sol-gel method has greater advantages, which include high purity, the low temperature required for synthesis, and excellent homogeneity of nanoparticles [27, 28]. TiO_2 nanoparticles also exhibit potent antibacterial properties that are useful in many biological applications. Recently, there are increasing research in alkali metal ion (Al, Ca, Ce, Co, Cu, Fe, Ga, In, Mn, Mg, Nb, Sn, and Sr) doping method, which leads to change in physical and chemical properties of TiO_2 nanoparticles and enhances the antibacterial applications [29]. Among these metals, Mg-TiO₂ NPs exhibit potent antibacterial activity, because Mg^{2+} can be substituted into the Ti^{4+} ion owing to their smaller ionic radii. The smaller ionic radii of Mg^{2+} ion helpful to enhance the antibacterial efficiency [30]. The efficiency of antibacterial activity also depends on the structure of microbes.

Matsunaga et al. [31] reported that TiO_2 nanoparticles showed good antimicrobial activity against *Escherichia coli* under UV irradiation. To overcome the drawbacks transition metals are doped to enhance the antibacterial efficiency under visible light. Karunakaran et al. [32] demonstrated that Cu doped TiO_2 nanoparticles effective antibacterial activity towards *E. coli* and *S. aureus* under visible light. Meanwhile, they also studied Ni-TiO₂ NPs against gram-positive and gram-negative bacteria. Hamal et al. [33] reported that Ag-doped TiO_2 nanoparticles enhance antibacterial activity against *E. coli* and *B. subtilis* and suggesting that the Ag is responsible for the enhancement of antibacterial efficiency. According to earlier reports, few works have been carried out on the effect of TiO_2 nanoparticles on antimicrobial activity [34].

Sahar Zinatloo-Ajabshir et al. [35] reported that the dysprosium stannate nanoparticles was synthesized by using Ficus

carica extract and applied as novel kind of visible light sensitive photocatalyst for efficient removal and destructive of organic contaminants in water. Saeed Moshtaghi et al. [36] exhibited that the nanocrystalline barium stannate was synthesized by simple coprecipitation method and also examined degradation of erythromycin dye as water pollutant. Sahar Zinatloo-Ajabshir et al. [37] described that the $\text{Nd}_2\text{Sn}_2\text{O}_7$ nanostructures was synthesized by using date palm extract and explored electrochemical hydrogen storage through chronopotentiometry way and the discharge capacity of synthesized sample of around 4013 mA h/g. Sahar Zinatloo-Ajabshir et al. [38] reported that the $\text{Dy}_2\text{Sn}_2\text{O}_7$ nanostructures was synthesized by using banana juice and also investigated the electrochemical hydrogen storage through chronopotentiometry method and the discharge capacity of synthesized sample of around 4023 mA h/g after 20 cycles.

However, to the best of our knowledge, only a few works have been reported on the antibacterial and Photocatalytic activity of Mg- TiO_2 NPs with different dopant concentrations. Arrak Klinbumrung et al. [39] reported the antibacterial activity for gram positive bacteria (*S.aureus*) only microwave assisted method, but our work reported both gram positive and gram negative bacteria by simple sol gel method. Moreover, Mg-TiO₂ NPs increase the concentration of oxygen species (ROS), and this oxygen species leading to the death of bacterial cells. The antibacterial activity of Mg-TiO₂ NPs depends on the variation in the doping concentration of Mg and the nature of bacterial species.

Herein, undoped and Mg-TiO₂ NPs were synthesized via the simple sol-gel method. The synthesized nanoparticles were investigated for structural, morphological, optical, antibacterial, and photocatalytic activity. The effect of various concentrations of Mg on the synthesis of Mg- TiO_2 NPs against gram-positive and gram-negative bacteria under visible light. The photocatalytic degradation efficiency of Mg-TiO₂ NPs for Methylene Blue under UV irradiation was also studied.

2 Experimental Sections

2.1 Preparation of Undoped and Mg-TiO₂ NPs

Chemicals were analytical grade and no need to further purification.

S.No	Chemical name	Chemical formula	Purification details	Company
1	Titanium (IV) Isopro- poxide	$\text{Ti(OCH(CH}_3)_2}_4$	99.9%	Merck Scientific company, India

S.No	Chemical name	Chemical formula	Purification details	Company
2	Magnesium nitrate hexahydrate	$\text{Mg}(\text{NO}_3)_2 \cdot 6\text{H}_2\text{O}$	99.8%	Merck Scientific company, India
3	Sodium hydroxide	NaOH	99.9%	Nice Scientific company, Cochin, India

For the preparation of Mg-TiO₂ NPs, 0.2 mol % of Magnesium nitrate was prepared in 100 ml of deionized water. Subsequently, 5 ml of Titanium (IV) Isopropoxide was prepared in 100 ml of Isopropyl Alcohol. Then the aqueous solution of Magnesium nitrate was added drop wise to form a homogenous mixture. After that, aqueous NaOH solution was added dropwise to this homogenous mixture to form white precipitation. Then the homogenous mixture was stirred at room temperature. Further, a homogenous mixture could age for 24 h. and then the white precipitate was washed with ethanol and distilled water to remove unwanted impurities present in the solution. Then the solution was centrifuged, and the precipitate was dried at 120° C for 2 h and annealed at 450° C for 5 h to obtain Mg-TiO₂ NPs. The same procedure was followed for different concentrations of dopant Mg (0.3 mol %, 0.4 mol % and 0.5 mol %). The obtained samples were ground with pestle and mortar and stored in an airtight container. The annealed samples were used for further studies. The same method was followed for TiO₂ nanoparticles without the addition of Magnesium nitrate.

2.2 Characterization

The prepared undoped and Mg-TiO₂ NPs were examined using the following characterization techniques. UV–Visible absorption spectroscopy was obtained in the wavelength range 200–800 nm using a UV visible spectrophotometer (JASCO-V-770 Spectroscopy). Fourier transform infrared spectroscopy (FTIR) was carried out by using Bruker Alpha FTIR spectrometer at a wavenumber range of 400 cm⁻¹–4000 cm⁻¹. Photoluminescence spectroscopy of the prepared samples was analyzed using an FP-3800 spectrofluorometer. XRD diffraction pattern was analyzed using Bruker D8 Advance X-ray diffractometer with $\text{CuK}\alpha 1$ ($\lambda = 1.54060 \text{ \AA}$) and $\text{CuK}\alpha 2$ ($\lambda = 1.54443 \text{ \AA}$) radiation operating at 30 mA and 45 kV at 2θ range of 10° to 90°. The Surface morphology of Mg-TiO₂ NPs was analyzed using a Field emission scanning electron microscope (SIGMA HV-CARL ZEISS) and HRTEM images were taken in

(JEOL – JEM -2010, JAPAN) with an accelerating voltage of 200 kV.

2.3 Antibacterial Experiment

E.Coli, *Pseudomonas aeruginosa*, *Bacillus sp* and *Staphylococcus aureus* were chosen as microbes for antibacterial assays. The antibacterial activity of undoped and Mg-TiO₂ NPs was tested using the disc diffusion method.

In brief, the microbes were cultivated in Müller-Hinton broth at 35 °C ± 2 °C on detour shuddering incubator (Remi, India) at 160 rpm. A pasture of microbial culture was arranged by dispersion of 10 mL culture broth of all test microbes on dense nutrient agar plates. The dishes were permitted to stand for 10–15 min for culture absorption. The 5 mm size discs/wells were perforated into the agar with the dome of sterilized micropipette tips. Using a spatula, 100 µg of undoped and Mg-TiO₂ NPs were kept into each of the discs on all plates. The microbes were inoculated to the culture media by inoculation in the petri dishes and incubated at 35 ± 2 °C for 24 h for culturing bacteria. After incubation, the diameter of zone of inhibition were examined.

2.4 Photocatalytic Degradation Study

UV light irradiation of Photocatalytic degradation of undoped and Mg-TiO₂ NPs was analyzed for Methylene blue dye. In a typical photo degradation analysis, 50 ml of methylene blue (40 mg /L) solution was mixed with the appropriate amount of prepared samples (undoped and Mg-TiO₂ NPs) and stirred well in a glass beaker. The obtained suspension was kept under darkroom for 30 min and then irradiated with UV light with constant stirring. 3 ml aqueous solution was extracted from the obtained suspension under UV irradiation with equal intervals of time. The absorption spectra of the solution were analyzed by UV visible spectrophotometer (JASCO-V-770 Spectroscopy). The photocatalytic rate constant for Methylene blue of prepared samples were calculated using the first-order equation

$$\ln (A_0/A) = kt \quad (1)$$

where A_0 is the initial absorption, A is the absorption after a time t and k is the first-order rate constant.

3 Result and Discussion

3.1 Structural Determination and Purity

XRD pattern of undoped and Mg-TiO₂ NPs exhibited peaks with tetragonal anatase phase reflections (JCPDS Card no. 78–2486) and possesses pure crystalline nature with trigonal

planar O-3 and Ti-6 Octahedral coordination geometry [40]. Figure 1 illustrates the XRD pattern of undoped and Mg-TiO₂ NPs with different concentrations of Mg under the same condition. The patterns are recorded in 2θ in the range of 20°–80°. The characteristics 2θ values are 25.30°, 32.65°, 37.59°, 47.86°, 53.81°, 55.09°, 62.57°, 68.78°, 70.30°, 75.37° and corresponding hkl plane values are (1 0 1), (0 0 2), (0 0 4), (2 0 0), (1 0 5), (2 1 1), (2 0 4), (1 1 5), (2 2 0) and (2 1 5) respectively. The prominent peak at 25° indicates the crystalline nature of prepared samples. The tetragonal anatase crystalline nature of TiO₂ remains unaffected with the amalgamation of Mg into TiO₂ lattice. When increasing the doping concentration Mg, the difference in the intensity of the diffraction peaks and minor shifts in the peak occurs this indicates the reduction of crystallite size and increase of volume of unit cell. The ionic radii of Mg²⁺ (0.71 Å) ion and Ti4+ (0.62 Å) are very near with each other, hence Mg²⁺ can easily enter the TiO₂ lattice [41]. The similar ionic radii of dopant arise the possibility of Mg²⁺ enter the TiO₂ lattice through substitution mode. Thereby, doping through the substitution model involves the direct substitution of metal ions to occupy their position in the lattice. The peak broadening and no impurity peak occur when increasing the dopant concentration Mg, which indicates a reduction of crystallite size, and all the dopant elements cannot enter into the TiO₂ lattice and some of them are formed on the surface of TiO₂ NPs.

The Scherrer's formula was used to calculate the crystallite size of undoped and Mg-TiO₂ NPs as follows [42],

$$D = k\lambda / \beta \cos \theta \quad (2)$$

where K is the Scherrer's constant, β is the full wave half maximum (FWHM) of the X-ray diffraction (radians), λ is

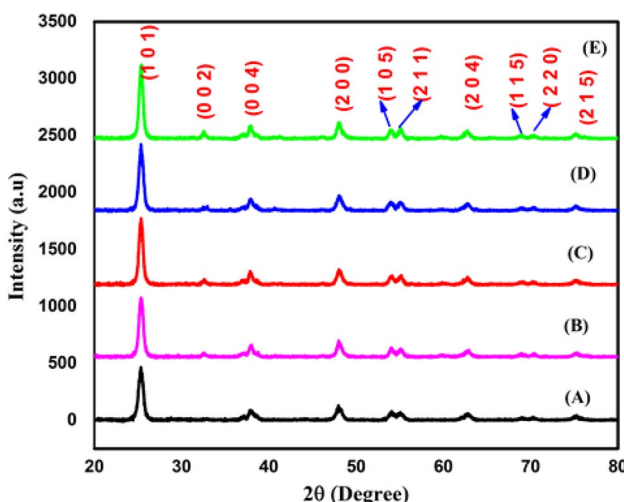


Fig. 1 XRD spectra of (A) undoped and Mg-TiO₂ NPs (B) 0.2 mol% (C) 0.3 mol% (D) 0.4 mol % (E) 0.5 mol % of Mg

the wavelength of the X-ray (nm) and θ is the diffraction angle. The assessed crystallite size of as-prepared nanoparticles was found to be 22 nm, 21 nm, 20.4 nm, 20 nm, and 19.6 nm respectively. The crystallite size is found to decrease with Mg-TiO₂ NPs increases which are due to Mg²⁺ ion is incorporated into the TiO₂ lattice. The doping with Mg with TiO₂ also increases the oxygen species and these oxygen species are responsible to enhance the antibacterial and photocatalytic activity.

The lattice constant of the tetragonal anatase phase of undoped and Mg-TiO₂ NPs was calculated using the formula,

$$\frac{1}{d^2} = \frac{h^2 + k^2}{a^2} + \frac{l^2}{c^2} \quad (3)$$

where d is the interplanar spacing, a and c are lattice constants, h k and l are the miller indices. Positional parameter (u), bond length (l), and volume of the unit cell (V) of as-prepared samples were obtained using the following relation.

$$V = a^2 c \text{ Å}^3 \quad (4)$$

$$L = \sqrt{\frac{a^2}{3} + (\frac{1}{2} - u)^2 c^2} \quad (5)$$

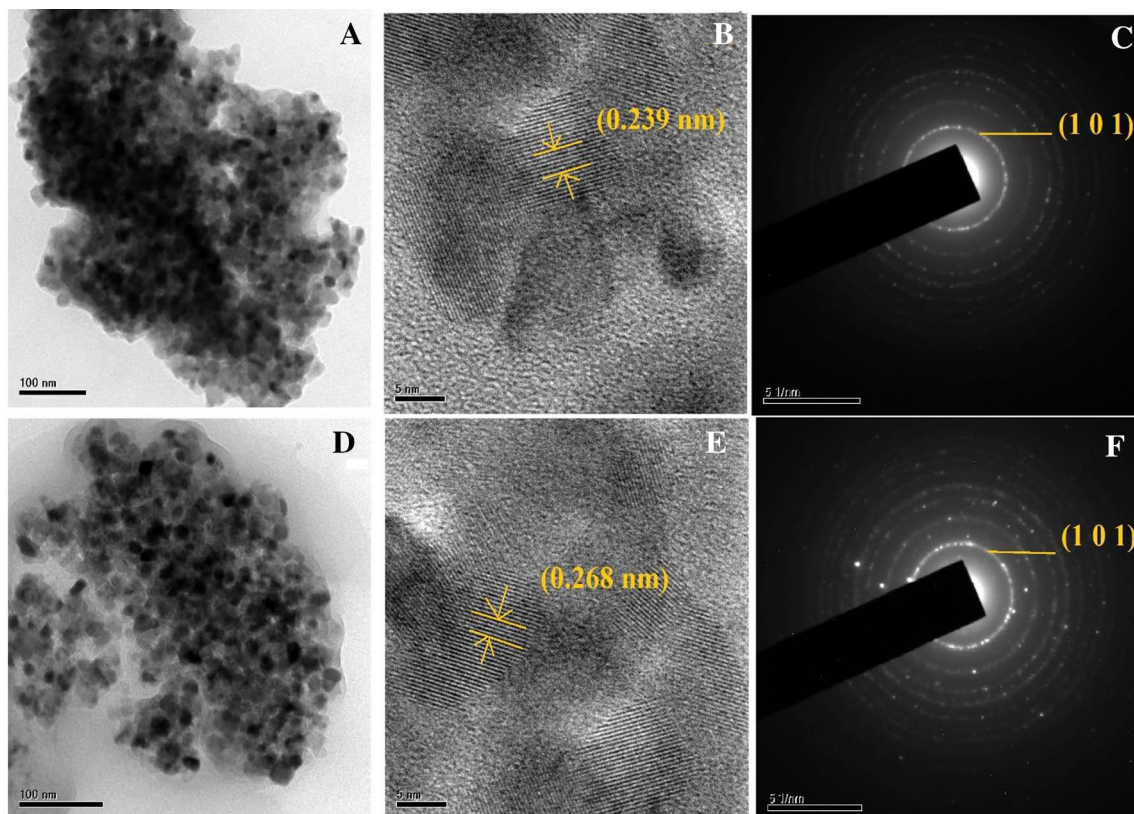
$$u = \frac{a^2}{3c^2} + 0.25 \quad (6)$$

The obtained value of crystallite size, lattice parameter, positional parameter, bond length, and unit cell volume of undoped and Mg-TiO₂ NPs are summarized in Table 1. As presented in Table 1, the crystallite size of as-prepared nanoparticles decreases when increases the dopant concentration Mg and also a slight variation in the positional parameter, bond length, and volume of the unit cell values, this might be due to the incorporation of Mg²⁺ ion into the TiO₂ lattice.

The different modes of vibration of as-prepared nanoparticles and chemical purity can be studied by using Fourier Transforms Infrared Technique (FTIR) and depicted in Fig. 2. The broadband at 3748 cm⁻¹ could be attributed to the hydroxyl group of stretching mode of vibration of TiO₂ nanoparticles and forms oxygen vacancies in the occurrence of water. The presence of the OH group also increases the photocatalytic activity since the OH group helps as a scavenger for photogenerated charge carriers [43]. The absorption band at 2936 cm⁻¹ and 2348 cm⁻¹ related to symmetric and asymmetric vibration of –CH₂ and –CH₃ groups. The band at 1626 cm⁻¹ related to characteristics of amide I and II and indicating the formation of the band at an infrared region which increases the surface hydroxylation of TiO₂ nanoparticles when doping

Table 1 Structural parameters of undoped and Mg-TiO₂ NPs

Sample	Crystallite size (nm)	a	c	c/a ratio	Positional parameter (u)	Bond length (l) Å	Volume of the unit cell (V) Å ³
TiO ₂	22	3.635	9.461	2.602	0.287	2.790	125.01
0.2 g of Mg	21	3.656	9.432	2.579	0.285	2.792	126.07
0.4 g of Mg	20.4	3.668	9.432	2.571	0.285	2.789	126.90
0.6 g of Mg	20	3.679	9.450	2.568	0.284	2.783	127.90
0.8 g of Mg	19.6	3.688	9.428	2.564	0.283	2.782	127.53

**Fig. 2** TEM analysis of **A** undoped and Mg-TiO₂ NPs, **B** 0.2 mol%, **C** 0.3 mol%, **D** 0.4 mol%, **E** 0.5 mol% of Mg

with Mg. FTIR band includes 1544 cm⁻¹ corresponds to C–N stretching modes of vibration. The peak at 1358 cm⁻¹ resembles to C–H stretching vibration [44–46]. The absorption peak appears at 468 cm⁻¹ corresponds to Ti–O stretching modes of vibration or antisymmetric Ti–O–Ti modes of vibration of TiO₂ nanoparticles. This peak plays a significant role in enhancing photocatalytic activity.

3.2 Optical Properties and Bandgap Assessment

The optical properties of as-prepared nanoparticles were examined using UV–visible absorption spectroscopy carried out at room temperature and depicted in Fig. 3.

Generally, TiO₂ nanoparticles tend to absorb UV light of bandgap 3.2 eV. The absorption peak exhibit UV cutoff wavelength which is attributed to photoexcitation of electron from the valence band (formed from 2p orbital of the oxide anion) to conduction band (formed from the 3d orbitals of the Ti⁴⁺ cation [47]). The shift in the absorption edge was observed for Mg-TiO₂ NPs which are ascribed to the acceptor tendency of Mg in the TiO₂ and creation of additional state within the TiO₂ lattice which leads to reducing the bandgap.

To estimate the bandgap of as-prepared samples, Tauc's formula is used from UV visible spectra [48].

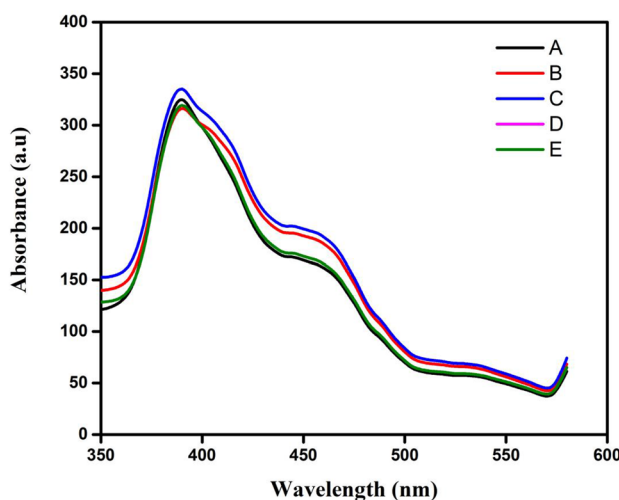


Fig. 3 PL analysis of (A) undoped and Mg-TiO₂ NPs (B) 0.2 mol% (C) 0.3 mol% (D) 0.4 mol% (E) 0.5 mol% of Mg

$$(\alpha h\nu) = A(h\nu - E_g)^n \quad (7)$$

where α - is the linear absorption coefficient, $h\nu$ is the energy of a photon; A is the proportionality constant and E_g is the bandgap energy respectively. Here n is the characteristics of transition in a semiconductor nanoparticle. And $n=1/2$ for direct bandgap and $n=2$ for indirect bandgap. The bandgap values of undoped and Mg-TiO₂ NPs were achieved by scheming a linear region in the plots $(\alpha h\nu)^{1/2}$ to the crossing with energy axis (E/eV) and shown in Fig. 4. The estimated bandgap energy of TiO₂ nanoparticles is 3.57 eV and bandgap energy values decrease from 3.57 eV to 3.54 eV respectively. The decrease in bandgap due to an increase in photo absorption and this might be enhancing the photocatalytic activity.

The structural defects and crystal properties of as-prepared samples were analyzed using PL analysis with an excitation wavelength of 345 nm at room temperature. Photoluminescence (PL) spectra of undoped and Mg-TiO₂ NPs depicted in Fig. 5. PL spectra exhibit a peak at 388 nm, 458 nm, and 535 nm respectively. There is no new peak arises for Mg-TiO₂ NPs. The prominent peak at 388 nm is due to UV emission and self-blocking excitons near the band edge of TiO₂. The UV emission band arises due to the recombination of electron–hole pair which is near band edge emission (NBE). The intensity of the peak slightly increases when Mg added to TiO₂ which is due to an increase in electron–hole pair recombination. The shifts in peak also due to a decrease in particle size and bandgap energy of as-prepared nanoparticles. The highest peak at 388 nm also confirms the formation crystalline nature of TiO₂. Another peak at 458 nm due to deep level emission from the structural defects such as oxygen vacancies and impurities on

the surface of TiO₂ [49]. PL spectra were observed between 300 and 550 nm this might be due to intrinsic and extrinsic structural defects. This may because when an electron from the valence band to the conduction band and forms the electron–hole pair. The low-intensity peak at 535 nm corresponds to green emission and it can be arising due to charge carriers formed after the recombination process take place and oxygen species on the surface of TiO₂ nanoparticles. The increase in oxygen vacancies happens with increasing dopant Mg and this may cause development in photocatalytic activity.

3.3 Morphology and Elemental Analysis

The surface morphology of the as-prepared undoped and Mg-TiO₂ NPs was examined using FESEM analysis and results are shown in Fig. 6. The morphology of as-prepared nanoparticles shows a spherical shape. The particle size of undoped and Mg-TiO₂ NPs is around 25 nm. From the XRD results, it can be inferred that the crystallite size is less than the particle size and it proves that the prepared nanoparticle is in crystalline nature. In addition, the aggregation and agglomeration occur in the prepared nanoparticles and it is shown in the FESEM images. The decrease in agglomeration can be attributed to the increasing the dopant concentration Mg and particle size also decreases. The crystalline is defined as the lowest even crystallographic unit based on the disorientation of the adjacent atoms and the nanoparticle consists of more than one crystalline with dissimilar direction. Here, particle size obtained from FESEM results is in good agreement with XRD results and this also actually happens in the case of nanoparticles. The high crystalline nature of prepared nanoparticles enhances the antibacterial and photocatalytic activity.

The quantitative microanalysis of undoped and Mg-TiO₂ NPs was analyzed by EDAX and shown in Fig. 7 and the results are listed in Table 2. The results from the EDAX spectra confirm the presence of Mg, Ti, and O and the percentage of Mg increases with increasing the dopant concentration, thereby decreasing the concentration of Ti into the TiO₂ lattice. Furthermore, the percentage of Mg and Ti indicates the substitution mode of doping on the surface of the TiO₂ lattice. The results also show that the increase in the percentage of oxygen on the surface of TiO₂ attributed to enhances the antibacterial and photocatalytic activity. No other additional impurities are detected in the EDAX spectra.

Figure 8(A-B) depicts the TEM analysis of undoped and Mg-TiO₂ NPs. The results illustrate the prepared nanoparticles are spherical. The entire prepared sample shows a uniform spherical morphology with well crystalline nature. Figure (C-D) indicates the lattice fringes of undoped and

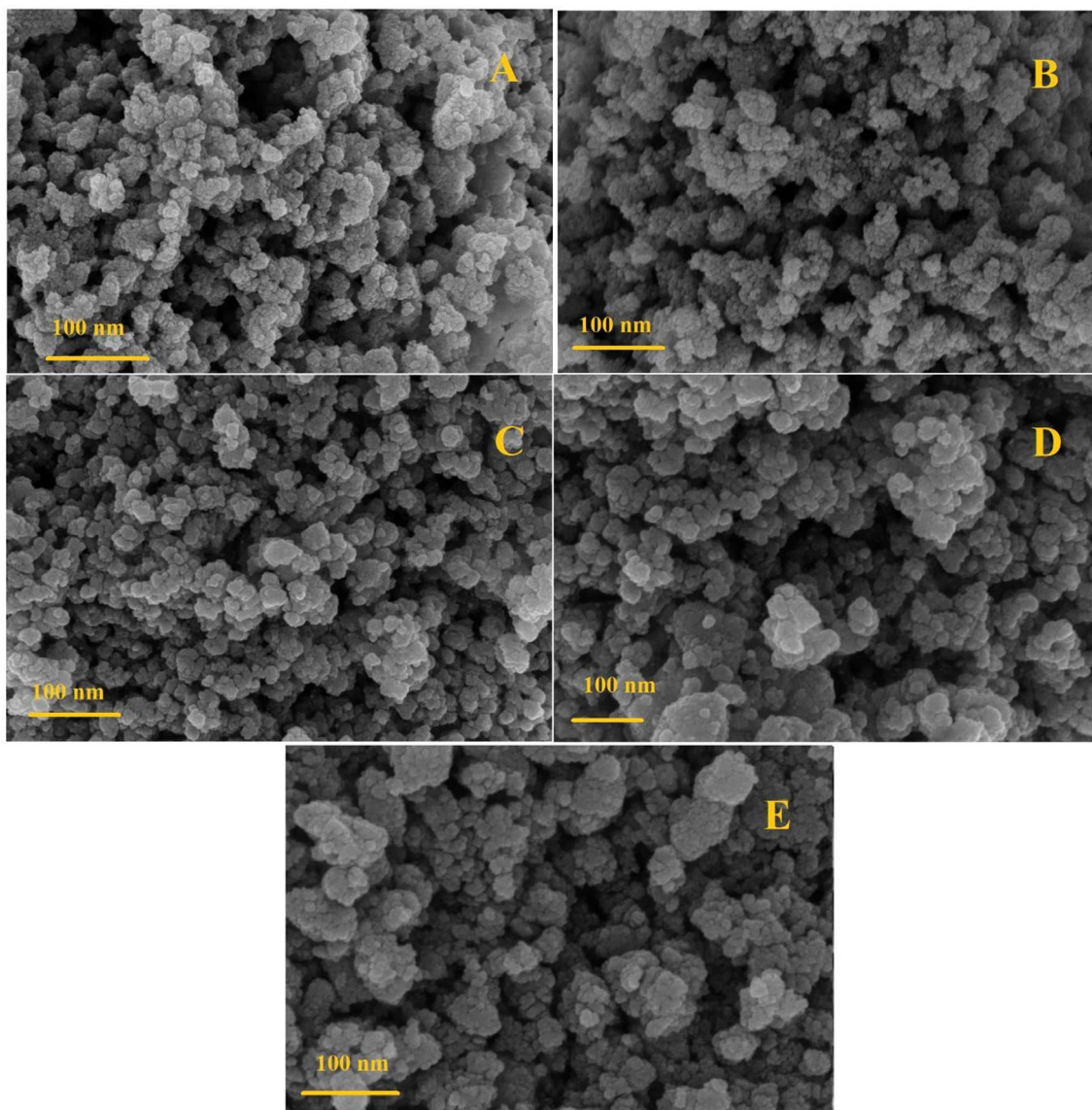


Fig. 4 FESEM analysis spectra of **A** undoped and Mg-TiO₂ NPs, **B** 0.2 mol%, **C** 0.3 mol%, **D** 0.4 mol%, **E** 0.5 mol% of Mg

Mg-TiO₂ NPs. d-spacing values are calculated using the relation [50].

$$Ll = dR \quad (8)$$

where L is the camera length (120 nm), l is the wavelength of the electron beam and R is the radius diffraction ring respectively. d—spacing values of undoped and Mg-TiO₂ NPs were found to be 0.239 nm and 0.268 nm respectively which corresponds to the (1 0 1) tetragonal anatase phase of TiO₂ nanoparticles. Lattice spacing values were found to be slight increases when Mg-TiO₂ NPs which are ascribed to the imperfections in TiO₂ lattice due to metal ion doping [51]. The intensity of the crystalline phase of TiO₂ nanoparticles was decreased which are well-matched with intensity peaks of XRD results. The crystallinity of as-prepared samples was

assessed using the selected area diffraction pattern (SAED) and portrayed in Fig. 8 (E–F). The ring pattern confirms the anatase crystalline nature of as-prepared nanoparticles and a bright spot indicates the formation of high crystallinity nature of undoped and Mg-TiO₂ NPs (1 0 1) anatase phase. The mean particle size of undoped and Mg-TiO₂ NPs was obtained to be 24.6 nm and 21.9 nm respectively. The assessed particle size is in good accord with the crystalline size of XRD results. From the TEM results, particle size decreases the increasing the dopant concentration which is due to Mg²⁺ ion is incorporated into the TiO₂ lattice. The smaller particle size improves photocatalytic activity.

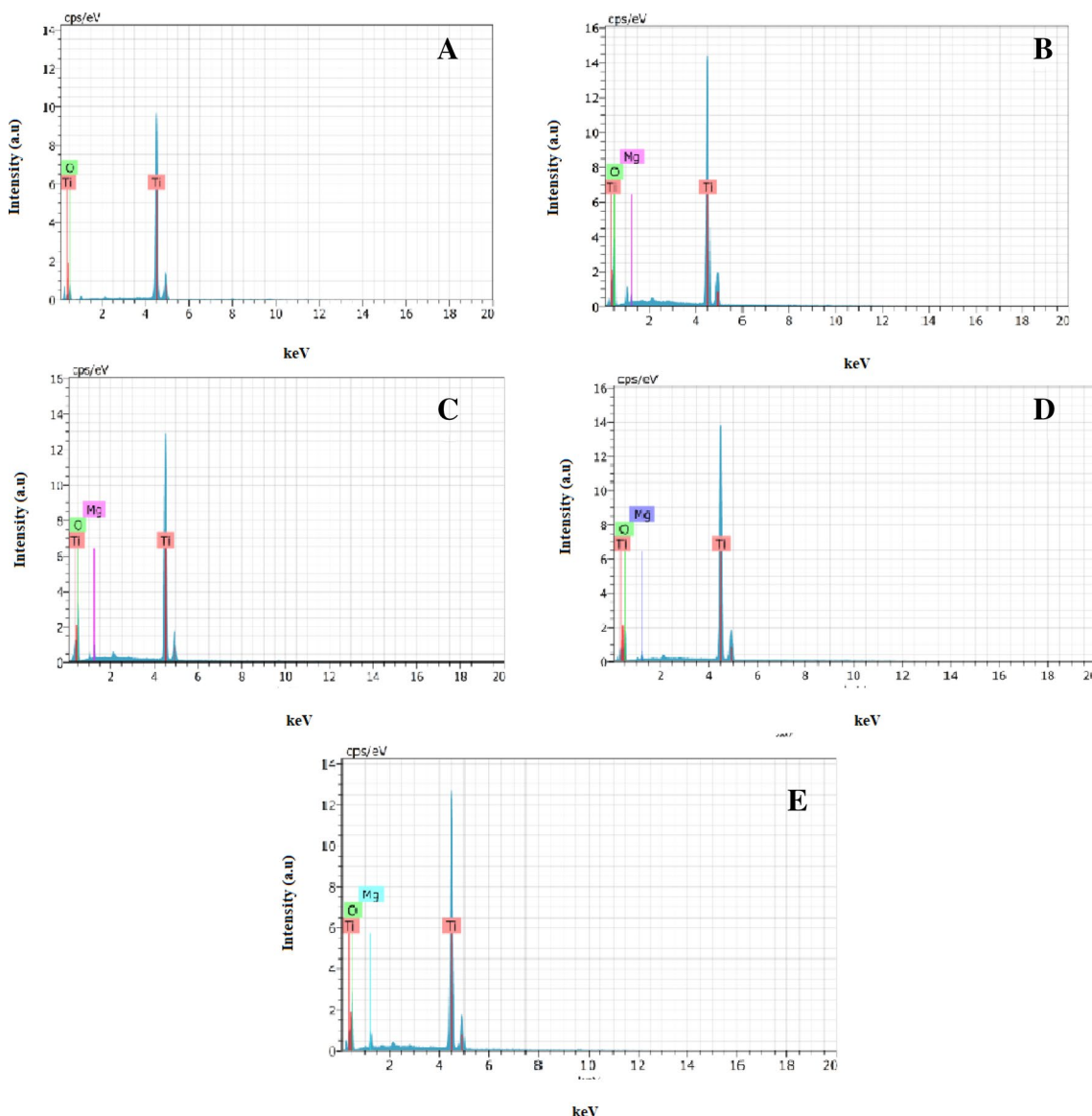


Fig. 5 EDAX analysis of **A** undoped and Mg-TiO₂ NPs, **B** 0.2 mol%, **C** 0.3 mol%, **D** 0.4 mol%, **E** 0.5 mol% of Mg

4 Antibacterial Activity

Generally, the antibacterial activity of nanoparticles depends on various factors such as phase formation, particle size, surface morphology, specific surface area, chemical composition, and surface hydroxyl groups [52, 53]. The antibacterial activities of Pure and different concentrations of Mg-TiO₂ NPs were investigated against *E.Coli*, *Pseudomonas aeruginosa*, *Bacillus sp* and *Staphylococcus aureus* by disc diffusion method. The zone of inhibition was increased when increasing the doping concentration Mg as shown in Fig. 9. Mg-TiO₂ NPs (0.5 mol%) exhibited the best antibacterial activities of both gram-negative and gram-positive bacteria as shown in Fig. 10. Moreover, gram-negative bacteria are

comparatively more sensitive to Mg-TiO₂ NPs than gram-positive bacteria. This might be due to the difference in the cell structure of bacteria. As the gram-positive bacteria have a thick lipopolysaccharide cell membrane as related to gram-negative bacteria. And lipopolysaccharide cell membrane acts as an additional barrier for undoped and Mg-TiO₂ NPs, leading to relatively lower antibacterial activities for gram-positive bacteria.

The several killing mechanisms of TiO₂ nanoparticles explained in literature such as ROS generation, superficial tension leads to cell damage, Ti²⁺ ion penetrates cell membrane leads to damage of cell wall, hole creation, and leakage of intracellular electrolytes [54, 55]. Amongst, ROS creation was mostly used to describe the antibacterial activities

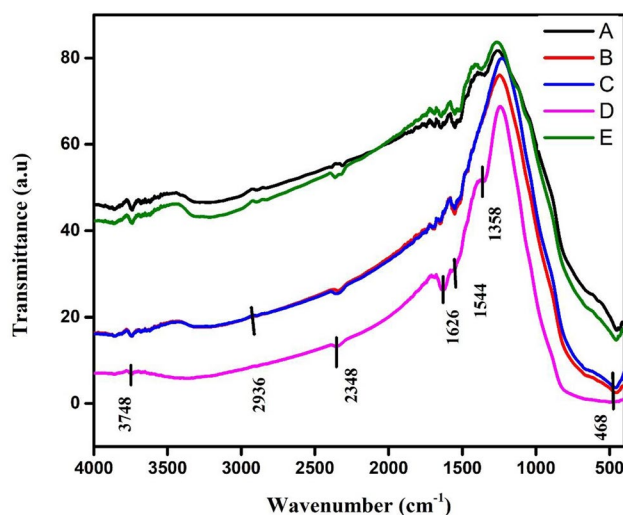


Fig. 6 FTIR analysis of (A) undoped and Mg-TiO₂ NPs B, (B) 0.2 mol%, (C) 0.3 mol%, (D) 0.4 mol%, (E) 0.5 mol % of Mg

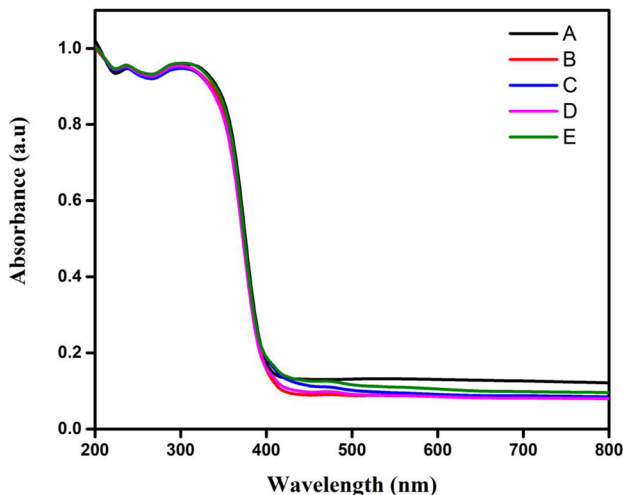


Fig. 7 UV analysis of (A) undoped and Mg-TiO₂ NPs, (B) 0.2 mol%, (C) 0.3 mol%, (D) 0.4 mol%, (E) 0.5 mol % of Mg

of TiO₂ nanoparticles. According to the ROS creation of TiO₂ nanoparticles, additional electron–hole pairs might be formed on the surface of nanoparticles. ROS creation mainly

consists of hydroxyl radicals, hydrogen peroxide (H₂O₂), and superoxide anion radicals [56]. Furthermore, TiO₂ nanoparticles bind with the external microbial membrane and enter the cell wall. This damage the cell wall, DNA, lipids, and protein synthesis and leads to bacteria viability [57]. The killing mechanism of TiO₂ nanoparticles is given below [58].



Carol López de Dicastillo et al. [59] reported the higher antibacterial activity of TiO₂ nanosphere against *Escherichia coli* and *Staphylococcus aureus*. Zimbone et al. [60] reported the antibacterial activity of TiO₂ nanoparticles against gram-negative bacteria *Escherichia coli*. The antibacterial activities of undoped and Mg-TiO₂ NPs also depend on the crystallite and morphology. The efficacy of antibacterial activities of undoped and Mg-TiO₂ NPs are shown in Table 1. The results reveal that antibacterial activities of Mg-TiO₂ NPs are higher for gram-negative bacteria than gram-positive bacteria. When increasing the concentration of Mg, the antibacterial activities also increase.

In this study, Mg-TiO₂ NPs (0.5 mol%) exhibited higher antibacterial activity because of the smaller crystallite size with a larger surface area. In addition, Mg also increases the oxygen vacancies in ROS generation to enhance the antibacterial activity. The doping of Mg with TiO₂ nanoparticles leads to the variation in particle size, morphology, and solubility of Ti²⁺. The results reveal that Mg-TiO₂ NPs will be a promising candidate for a potential drug delivery system to cure some significant infections in the future Table (3).

5 Photocatalytic Activities

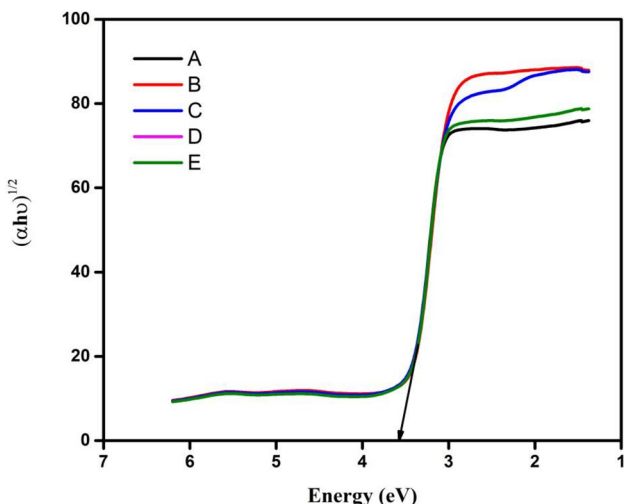
UV irradiated Photocatalytic degradation of Methylene Blue for undoped and Mg-TiO₂ NPs are depicted in Fig. 11. Mg-TiO₂ NPs show enhanced Photocatalytic degradation

Table 2 Elemental composition of undoped and Mg-TiO₂ NPs

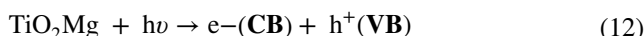
Sample	Wt%			At%		
	Ti	O	Mg	Ti	O	Mg
TiO ₂	71.82	28.58	–	45.51	54.49	–
0.2 g of Mg	52.55	46.75	0.70	27.11	72.28	0.71
0.4 g of Mg	50.90	47.81	1.30	25.90	72.80	1.30
0.6 g of Mg	52.80	45.64	1.60	27.43	70.96	1.60
0.8 g of Mg	54.48	43.83	1.68	28.83	69.42	1.68

Table 3 Antibacterial activity of undoped and Mg-TiO₂ NPs

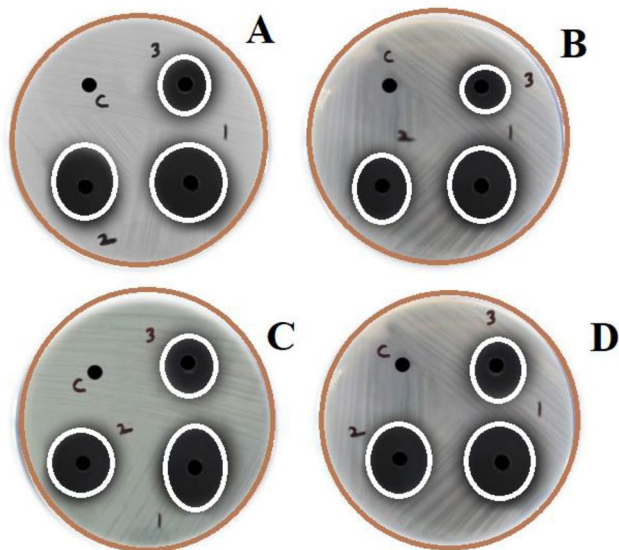
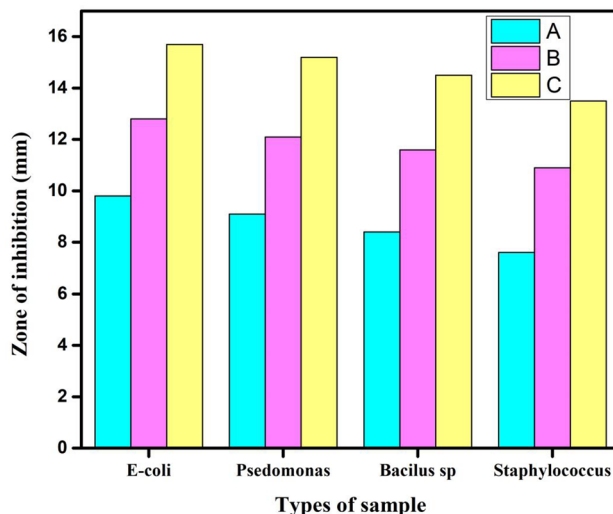
Organisms	Zone of inhibition (Diameter, mm)			
	Control	Synthesized nanoparticles		
		Pure TiO ₂	Mg-TiO ₂ (0.2 g)	Mg-TiO ₂ (0.8 g)
E-coli	7	9.8	12.8	15.7
Psedomonas	7	9.1	12.1	15.2
Bacillus sp	7	8.4	11.6	14.5
Staphylococcus	7	7.6	10.9	13.5

**Fig. 8** Tauc's plot of (A) undoped and Mg-TiO₂ NPs, (B) 0.2 mol%, (C) 0.3 mol%, (D) 0.4 mol%, (E) 0.5 mol% of Mg

efficiency than TiO₂ nanoparticles. The photocatalytic reactions are initiated from OH[·] and O²⁻ radicals formed on the surface of TiO₂ nanoparticles [61]. The photocatalytic mechanism of as prepared samples were shown in Fig. 12.



The Photocatalytic degradation efficiency of TiO₂ nanoparticles from 0 – 45 min was found to be 68%, 74%, and 86% and 76%, 88%, and 95% respectively for Mg-TiO₂ NPs. From the result of photodegradation efficiency, Mg-TiO₂ NPs exhibit potent performance than Pure TiO₂ nanoparticles. The higher photocatalytic efficiency for Mg-TiO₂ NPs due to smaller crystallite size and higher bandgap energy than TiO₂ nanoparticles. Because the crystallite size and bandgap energy play an important role in photocatalytic activity. And also dopant Mg modified the physical and chemical properties of TiO₂ nanoparticles. The reduced crystallite size of Mg-TiO₂ NPs nanoparticles also decreases the recombination of photogenerated electron–hole pair and

**Fig. 9** Zone of Inhibition of 1) undoped and 2) Mg-TiO₂ NPs (0.2 mol%) 3) Mg-TiO₂ NPs (0.5 mol%) (A) Bacillus subtilis, (B) Staphylococcus aureus, (C) Pseudomonas aeruginosa and (D) Klebsiella pneumonia**Fig. 10** Antibacterial activity of (A) undoped and (B) Mg-TiO₂ NPs (0.2 mol%) (C) Mg-TiO₂ NPs (0.5 mol%)

it also enhances the photocatalytic activity. The higher concentration of Mg-TiO₂ NPs shows enhanced photocatalytic activity than TiO₂ nanoparticles and this is because of the charge separation efficiency of electron–hole pair. And also, when Mg-TiO₂ NPs could form surface defects and oxygen species on the surface of prepared nanoparticles. The enhanced photocatalytic activity of Mg-TiO₂ NPs is due to smaller crystallite size and bandgap energy which was confirmed by XRD and UV analysis respectively. The calculated

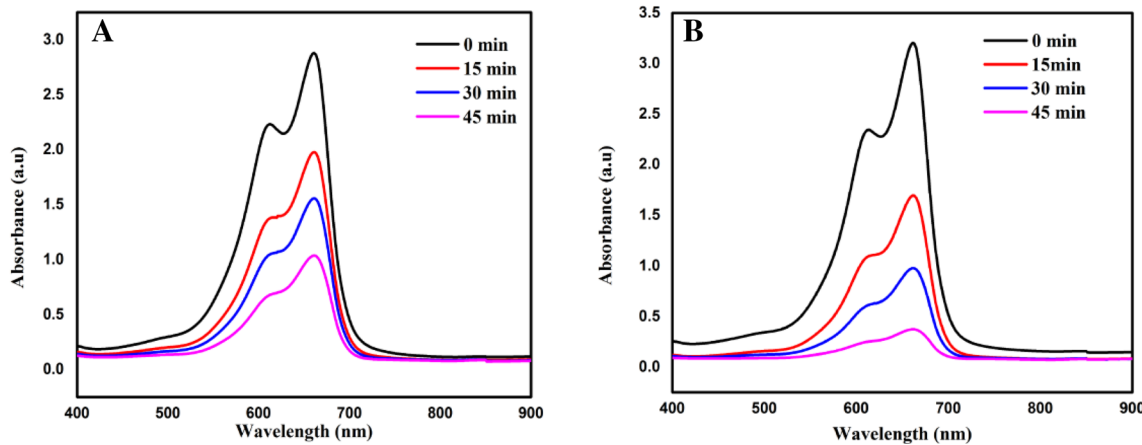
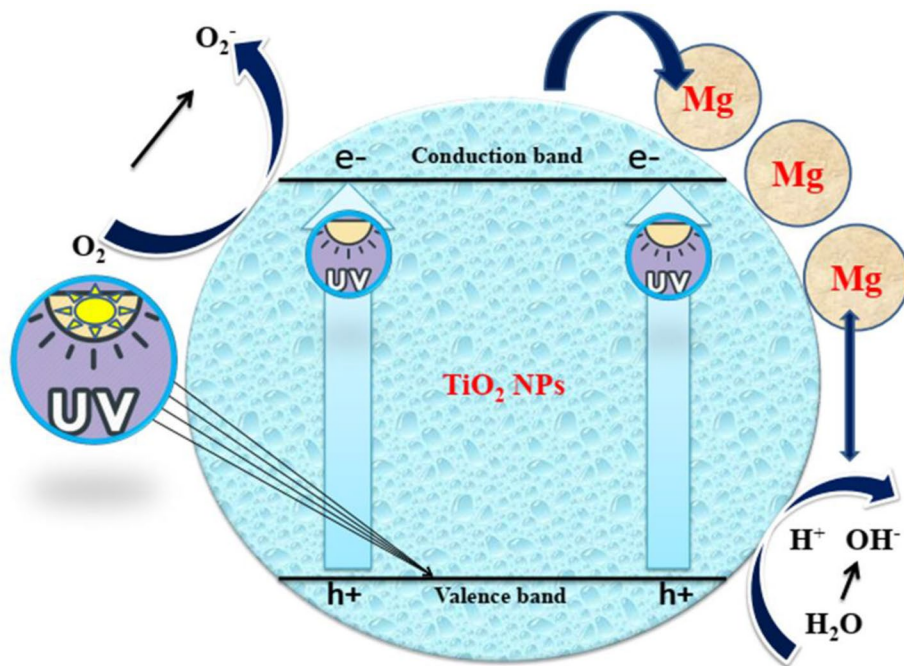


Fig. 11 Photocatalytic degradation of (A) undoped and (B) Mg-TiO₂ NPs (0.5 mol%)

Fig. 12 Photocatalytic mechanism of undoped and Mg-TiO₂ NPs



rate constant of TiO₂ nanoparticles were 0.023, 0.035, and 0.054 min⁻¹ after 45 min and 0.026, 0.038, and 0.059 min⁻¹ for Mg-doped TiO₂ were and shown in Fig. 13. The higher rate constant was obtained for Mg-doped TiO₂ nanoparticles and this is due to higher bandgap energy which causes higher redox potential for photogenerated electron–hole pair which extensively enhances the photocatalytic activity.

The photodegradation efficiency of undoped and Mg-TiO₂ NPs over 5 cycles for Methylene Blue over 45 min is shown in Fig. 14. The efficiency of TiO₂ nanoparticles was decreased from 86 to 76% and 95% to 92% for Mg-TiO₂ NPs. The lower efficiency of TiO₂ nanoparticles is due to the photo corrosion phenomenon during photocatalytic

reactions. On the other hand, doping with alkali metals increases the photocorrosive resistance and increases the chemical stability of TiO₂ nanoparticles during photocatalytic reactions. The photo corrosion phenomenon in the TiO₂ nanoparticles can be occur using the relations [62].



The photo corrosion is caused by the reaction of oxygen species and holes present on the surface of TiO₂ nanoparticles. According to XRD results, Mg-TiO₂ NPs leads to increases in the oxygen species and also increases the chemical stability of photocatalytic reactions.

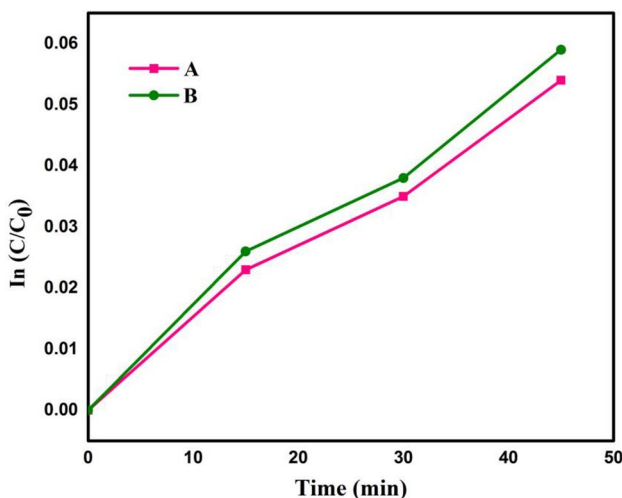


Fig. 13 Rate constant for (A) undoped and (B) Mg-TiO₂ NPs (0.5 mol%)

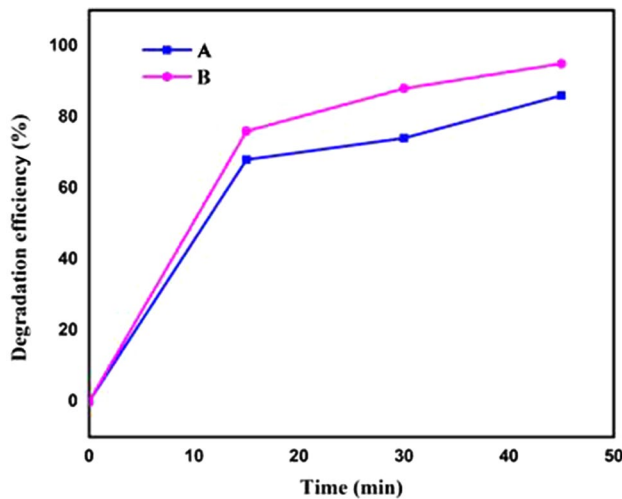


Fig. 14 Degradation efficiency of (A) undoped and (B) Mg-TiO₂ NPs (0.5 mol%) over 5 cycles for Methylene Blue

6 Conclusion

Bestowing to this work, undoped and Mg doped TiO₂ nanoparticles were synthesized by facile sol-gel technique. The synthesized nanoparticles were characterized by XRD, FESEM with EDAX, TEM, UV, FTIR and PL analysis. The XRD spectrum confirms the presence of tetragonal anatase phase of TiO₂ nanoparticles with lesser crystallite size. The crystallite size decreases from 22 nm to 19 nm with increasing the concentration of dopant Mg. FESEM and TEM analysis also confirms the various sized smooth spherical morphology of TiO₂ nanoparticles was

achieved from this method. EDAX analysis also confirms the presence of Ti, O and Mg without any other impurities. Red shift in UV analysis confirms the incorporation of Mg into TiO₂ nanoparticles. PL analysis confirms the UV emission and green emission region and change in intensity of the peak confirms the incorporation of Mg. The bandgap energy values decrease from 3.57 to 3.54 eV with Mg doping, resulting decreasing in crystallite size. The presence of functional group was confirmed by FTIR spectrum and stretching modes of vibration of TiO₂ nanoparticles was observed at 468 cm⁻¹. The prepared nanoparticles were also investigated for antimicrobial and photocatalytic activity. Pure and Mg doped TiO₂ nanoparticles show potent killing effect against the gram-negative bacteria than the gram-positive bacteria. The difference in killing effect due to cell structure and smaller crystallite size of prepared nanoparticles. Mg doped TiO₂ nanoparticles shows higher degradation efficiency than TiO₂ nanoparticles for Methylene Blue and this is because of smaller crystallite size. This method was a simple, cost effective, good dopant to preparation of low crystallite size TiO₂ nanoparticles.

References

1. K.S. Kavitha, S. Baker, D. Rakshith, H.U. Kavitha, H.C. Yashwantha Rao, B.P. Harini, Plants as green source towards synthesis of nanoparticles. *Int. Research J. Bio. Sci.* **2**, 66–77 (2013)
2. M. Abhilash, Potential applications of nanoparticles. *Int. J. Pharm. Biol. Sci.* **1**, 1–12 (2010)
3. S. Nagarajan, K.K. Arumugam, Extracellular synthesis of zinc oxide nanoparticle using seaweeds of Gulf of Mannar, India. *J. Nanobiotechnol* **11**, 1–39 (2013)
4. A.S. Hameed, C. Karthikeyan, S. Sasikumar, V. Senthilkumar, S. Kumaresan, G. Ravi, *Journal of Materials Chemistry B* **1**, 5950–5962 (2013)
5. A.S. Hameed, C. Karthikeyan, V. Senthilkumar, S. Kumaresan, S. Sasikumar, *Mater. Sci. Eng., C* **52**, 171–177 (2015)
6. A.S. Hameed, C. Karthikeyan, A.P. Ahamed, N. Thajuddin, N.S. Alharbi, S.A. Alharbi, Ravi G *Scientific reports*. **6**, 24312 (2016)
7. A. Sirelkhatim, S. Mahmud, A. Seenii, N.H.M. Kaus, L.C. Ann, S.K.M. Bakhorii, H. Hasan, D. Mohamad, Review on zinc oxide nanoparticles: antibacterial activity and toxicity mechanism. *Nano-Micro Lett.* **7**, 219–242 (2015)
8. J.H. Li, R.Y. Hong, M.Y. Li, H.Z. Li, Y. Zheng, J. Ding, Effects of ZnO nanoparticles on the mechanical and antibacterial properties of polyurethane coatings. *Prog. Org. Coat.* **64**, 504–509 (2009)
9. S. Zinatloo-Ajabshir, S.A. Heidari-Asil, M. Salavati-Niasari, Simple and eco-friendly synthesis of recoverable zinc cobalt oxide-based ceramic nanostructure as high-performance photocatalyst for enhanced photocatalytic removal of organic contamination under solar light. *Sep. Purif. Technol.* **267**, 118667 (2021)
10. S. Zinatloo-Ajabshir, M. Baladi, Masoud Salavati-Niasari Enhanced visible-light-driven photocatalytic performance for degradation of organic contaminants using PbWO₄ nanostructure fabricated by a new, simple and green sonochemical approach. *Ultrason. Sonochem.* **72**, 105420 (2021)

11. S. Zinatloo-Ajabshir, Seyed Ali Heidari-Asil, Masoud Salavati-Niasari Recyclable magnetic ZnCo₂O₄-based ceramic nanostructure materials fabricated by simple sonochemical route for effective sunlight-driven photocatalytic degradation of organic pollution, *Ceramics International*, Volume 47, Issue 7. Part A 1, 8959–8972 (2021)
12. H.A. Alhadrami, F. Al-Hazmi, Antibacterial activities of titanium oxide nanoparticles. *J. Bioelectron. Nanotechnol.* **2**, 5 (2017)
13. S. Banu, V. Vishnu, K. Jamuna, G.A. Kurian, Physicochemical investigation and biovaluation of TiO₂ nanocrystals synthesized by chemical and green route. *Int. J. Pharm. Pharm. Sci.* **6**, 396–400 (2014)
14. P. Periyat, D.E. McCormack, S.J. Hinder, S.C. Pillai, One-pot synthesis of anionic (nitrogen) and cationic (sulfur) codoped high-temperature stable, visible light active, anatase photocatalysts. *J. Phys. Chem. C* **113**, 3246–3253 (2009)
15. S. Zinatloo-Ajabshir, N. Ghasemian, M. Mousavi-Kamazani, M. Salavati-Niasari, Effect of zirconia on improving NO_x reduction efficiency of Nd₂Zr₂O₇ nanostructure fabricated by a new, facile and green sonochemical approach. *Ultrasound. Sonochem.* **71**, 105376 (2021)
16. S.A. Heidari-Asil, S. Zinatloo-Ajabshir, O. Amiri, M. Salavati-Niasari, Amino acid assisted-synthesis and characterization of magnetically retrievable ZnCo₂O₄–Co₃O₄ nanostructures as high activity visible-light-driven photocatalyst. *Int. J. Hydrogen Ener.* **45**(43), 22761–22774 (2020)
17. B.B. Muhammad, A. Javed, A. Irfana, Shahid, Effects of solvent on the structure and properties of titanium dioxide nanoparticles and their antibacterial activity. *Iran. J. Chem. Chem. Eng.* **38**(4), 261–272 (2019)
18. Q. Zhao, M. Wang, He. Yang, D. Shi, C.L. Yuzheng, K. Rahme, J.D. Holmes, M.A. Morris, N.K. Slater, Non-solvolytic synthesis of aqueous soluble TiO₂ nanoparticles and real-time dynamic measurements on the nanoparticle formation. *Nanoscale res. lett.* **7**, 1–10 (2012)
19. O.L. Kang, A. Ahmad, U.A. Rana, N.H. Hassan, Sol-gel titanium dioxide nanoparticles: preparation and structural characterization. *Journal of Nanotechnology* **2016**, 7 (2016)
20. A. Feinle, M.S. Elsaesser, N. Hüsing, Sol-gel synthesis of monolithic materials with hierarchical porosity. *Chem. Soc. Rev.* **45**, 3377–3399 (2016)
21. R. Desai, S.K. Gupta, P.K. Shree Mishra, A.P. Jha, The synthesis Of Tio₂ nanoparticles by wet-chemical method and their photoluminescence, thermal and vibrational characterizations: effect of growth condition. *Int. J. Nanosci.* **10**(6), 1249–1256 (2011)
22. W. Buraso, V. Lachom, P. Siriya, P. Laokul, Synthesis of TiO₂ nanoparticles via a simple precipitation method and photocatalytic performance. *Mater. Res. Express* **5**, 115003 (2018)
23. Hadja Fatima Mehnane, Changlei Wang, Kiran Kumar Kondamareddy, Wenjing Yu, Weiwei Sun, Haimin Liu, Sihang Bai, Wei Liu, Shishang Guo and Xing-Zhong Zhao, Hydrothermal synthesis of TiO₂ nanoparticles doped with trace amounts of strontium, and their application as working electrodes for dye sensitized solar cells: tunable electrical properties & enhanced photo-conversion performance. *RSC Adv.* **7**, 2358 (2017)
24. J.O. Carneiro, S. Azevedo, F. Fernandes, E. Freitas, M. Pereira, C.J. Tavares, S. Lanceros-Me'ndez, V. Teixeira, , Synthesis of iron-doped TiO₂ nanoparticles by ball-milling process: the influence of process parameters on the structural, optical, magnetic, and photocatalytic properties. *J Mater Sci* **49**, 7476–7488 (2014)
25. M.Y. Nassar, E.I. Alia, E.S. Zakaria, Tunable auto-combustion preparation of TiO₂ nanostructures as efficient adsorbents for the removal of an anionic textile dye. *RSC Adv.* **7**, 8034 (2017)
26. C. Jayaseelan, A.A. Rahuman, S.M. Roopan, A.V. Kirthi, J. Venkatesan, S.-K. Kim, M. Iyappan, C. Siva, Biological approach to synthesize TiO₂ nanoparticles using Aeromonas hydrophila and its antibacterial activity. *Spectrochimica. Acta. Part A: Mol. Biomol. Spec.* **107**, 82–89 (2013)
27. V.I. Kondratiev, I. Kink, A.E. Romanov, Low Temperature Sol-Gel Technique for Processing Al- Doped Zinc Oxide Films. *Mater. Phys. Mech.* **17**, 38–46 (2013)
28. Ullattil, S. G., & Periyat, P, Sol-Gel Synthesis of titanium dioxide. sol-gel materials for energy, *Environ. Electron. Appl.*, (2017), 271–283.
29. Wang, Preparation, characterization and the antimicrobial properties of metal ion-doped TiO₂ nano-powders. *Ceramic. Inter.* **44**, 5145–5154 (2018)
30. S. Shakir, Abd-ur -Rehman, H. M., Yunus, K., Iwamoto, M., & Periasamy, V., , Fabrication of un-doped and magnesium doped TiO₂ films by aerosol assisted chemical vapor deposition for dye sensitized solar cells. *J. Alloys. Comp.* **737**, 740–747 (2018)
31. T. Matsunaga, R. Tomoda, T. Nakajima, H. Wake, Photoelectrochemical sterilization of microbial cells by semiconductor powders. *FEMS Microbiol. Lett.* **29**, 211–214 (1985)
32. C. Karunakaran, G. Abiramasundari, P. Gomathisankar, G. Manikandan, V. Anandi, *J. Colloids Interface. Sci.* **352**, 68–74 (2010)
33. D.B. Hamal, J.A. Haggstrom, G.L. Marchin, M.A. Ikenberry, K. Hohn, K.J. Klabunde, *Langmuir* **26**, 2805 (2010)
34. B. Arora, M. Murar, V. Dhumale, Antimicrobial potential of TiO₂ nanoparticles against MDR *Pseudomonas aeruginosa*. *J. Exp. Nanosci.* **10**, 819–827 (2014)
35. S. Zinatloo-Ajabshir, Maryam Sadat Morassaei, Omid Amiri, Masoud Salavati-Niasari, Green synthesis of dysprosium stannate nanoparticles using *Ficus carica* extract as photocatalyst for the degradation of organic pollutants under visible irradiation. *Ceram. Int.* **46**, 6095–6107 (2020)
36. S. Moshtaghi, S. Zinatloo-Ajabshir, M. Salavati-Niasari, Nanocrystalline barium stannate: facile morphology-controlled preparation, characterization and investigation of optical and photocatalytic properties. *J Mater Sci: Mater Electron* **27**, 834–842 (2016)
37. S. Zinatloo-Ajabshir, Maryam Sadat Morassaei, Omid Amiri, Masoud Salavati-Niasari, Loke Kok Foong, Nd₂Sn₂O₇ nanostructures: Green synthesis and characterization using date palm extract, a potential electrochemical hydrogen storage material. *Ceram. Int.* **46**, 17186–17196 (2020)
38. S. Zinatloo-Ajabshir, Maryam Sadat Morassaei, Masoud Salavati-Niasari, Simple approach for the synthesis of Dy₂Sn₂O₇ nanostructures as a hydrogen storage material from banana juice. *J. Clean. Prod.* **222**, 103–110 (2019)
39. Arrak Klinbumrung, Panuwat Katekaew , Khuruwan Klinbumrung, Optical Characteristics and Antimicrobial Performance of Mg Doped TiO₂ Nanostructures Synthesized by Microwave Assisted Method, The Second Materials Research Society of Thailand International Conference AIP Conf. Proc. 2279, 120009–1–120009–7.
40. R.S. Dubey, S. Singh, Investigation of structural and optical properties of pure and chromium doped TiO₂ nanoparticles prepared by solvothermal method. *Results in Physics* **7**, 1283–1288 (2017)
41. J.O. Olowoyo, M. Kumar, N. Singhal, S.L. Jain, J.O. Babalola, A.V. Vorontsov, U. Kumar, Engineering and modeling the effect of Mg doping in TiO₂ for enhanced photocatalytic reduction of CO₂ to fuels. *Catal. Sci. Technol.* **8**, 3686–3694 (2018)
42. S.E. Arasi, J. Madhavan, M.V. Antony Raj, Effect of samarium (Sm³⁺) doping on structural, optical properties and photocatalytic activity of titanium dioxide nanoparticles. *J. Taibah Univ. Sci.* **12**, 186–190 (2018)
43. T. Ali, P. Tripathi, A. Azam, W. Raza, A.S. Ahmed, A. Ahmed, M. Munee, Photocatalytic performance of Fe-doped TiO₂nano particles under visible-light irradiation. *Materials Research Express* **4**, 015022 (2017)

44. A. Bokare, M. Pai, A.A. Athawale, Surface modified Nd doped TiO₂ nanoparticles as photocatalysts in UV and solar light irradiation. *Sol. Energy* **91**, 111–119 (2013)
45. M. Hudlikar, S. Joglekar, M. Dhaygude, K. Kodam, Green synthesis of TiO₂ nanoparticles by using aqueous extract of *Jatropha curcas* L. latex. *Mater. Lett.* **75**, 196–199 (2012)
46. A. León, P. Reuquen, C. Garín, R. Segura, P. Vargas, P. Zapata, P.A. Orihuela, FTIR and Raman characterization of TiO₂ nanoparticles coated with polyethylene glycol as carrier for 2-methoxyestradiol. *Appl. Sci.* **7**, 49 (2017)
47. Li. Xuemin, G. Zhengkai, He. Tao, The doping mechanism of Cr into TiO₂ and its influence on the photocatalytic performance. *Phys Chem Chem Phys* **15**, 20037–20045 (2013)
48. F.N. Jiménez-García, B. Segura-Giraldo, E. Restrepo-Parra, G.A. López-López, Synthesis of TiO₂ thin films by the SILAR method and study of the influence of annealing on its structural, morphological and optical properties. *Ingeniare. Revista chilena de ingeniería* **23**, 622–629 (2015)
49. R. Sharma, A. Sarkar, R. Jha, A.K. Sharma, D. Sharma, Sol-gel mediated synthesis of TiO₂ nanocrystals: structural, optical and electrochemical properties. *Int J Appl Ceram Technol.* **17**, 1400–1409 (2020)
50. G. Kasi, J. Seo, Influence of Mg doping on the structural, morphological, optical, thermal, and visible-light responsive antibacterial properties of ZnO nanoparticles synthesized via co-precipitation. *Mater. Sci. Eng. B* **98**, 717–725 (2019)
51. K. Mani Rahulan, S. Ganesan, P. Aruna, Synthesis and optical limiting studies of Au-doped TiO₂ nanoparticles. *Adv Nat Sci: Nanosci Nanotechnol* **2**, 025012 (2011)
52. B. Wu, R. Huang, M. Sahu, X. Feng, P. Biswas, Y.J. Tang, Bacterial responses to Cu-doped TiO₂ nanoparticles. *Sci. Total Environ.* **408**, 1755–1758 (2010)
53. T. Ali, A. Ahmed, U. Alam, P. Imran Uddin, M.M. Tripathi, Enhanced photocatalytic and antibacterial activities of Ag-doped TiO₂ nanoparticles under visible light. *Mater. Chem. Phys.* **212**, 325–335 (2018)
54. X. Jiang, L. Yang, P. Liu, X. Li, J. Shen, The photocatalytic and antibacterial activities of neodymium and iodine doped TiO₂ nanoparticles. *Colloids Surf., B* **79**, 69–74 (2010)
55. J. Ananpattarachai, Y. Boonto, P. Kajitvichyanukul, Visible light photocatalytic antibacterial activity of Ni-doped and N-doped TiO₂ on *Staphylococcus aureus* and *Escherichia coli* bacteria. *Environ. Sci. Pollut. Res.* **23**, 4111–4119 (2015)
56. Q. Zhao, M. Wang, H. Yang, D. Shi, Y. Wang, Preparation, characterization and the antimicrobial properties of metal ion-doped TiO₂ nano-powders. *Ceram. Int.* **44**, 5145–5154 (2018)
57. G.V. Anehosur, R.D. Kulkarni, M.G. Naik, R.K. Nadiger, Synthesis and determination of antimicrobial activity of visible light activated TiO₂ nanoparticles with polymethyl methacrylate denture base resin against *staphylococcus aureus*. *Anehosur J Gerontol Geriatric Res* **1**, 1000103 (2012)
58. M. Behpour, M. Chakeri, Ag-doped TiO₂ nanocomposite prepared by sol gel method: photocatalytic bactericidal under visible light and characterization. *JNS* **2**, 227–234 (2012)
59. Carol López de Castillo, Cristian Patiño, María José Galotto, Yesseny Vásquez-Martínez, Claudia Torrent, Daniela Alburquerque, Alejandro Pereira, and Juan Escrig, Novel hollow titanium dioxide nanospheres with antimicrobial activity against resistant bacteria. *Beilstein J. Nanotechnol.* **10**, 1716–1725 (2019)
60. M. Zimbone, M.A. Buccheri, G. Cacciato, R. Sanz, G. Rappazzo, S. Boninelli, M.G. Grimaldi, Photocatalytical and antibacterial activity of TiO₂ nanoparticles obtained by laser ablation in water. *Appl. Catal. B* **165**, 487–494 (2015)
61. R.P. Barkul, M.K. Patil, S.M. Patil, V.B. Shevale, S.D. Delekar, Sunlight-assisted photocatalytic degradation of textile effluent and Rhodamine B by using iodine doped TiO₂ nanoparticles. *J. Photochem. Photobiol., A* **349**, 138–147 (2017)
62. J.O. Olowoyo, M. Kumar, N. Singhal, S.L. Jain, J.O. Babalola, A.V. Vorontsov, U. Kumar, Engineering and modeling the effect of mg doping in TiO₂ for enhanced photocatalytic reduction of CO₂ to fuels. *J. Name.* **00**, 1–3 (2013)

Publisher's Note Springer Nature remains neutral with regard to jurisdictional claims in published maps and institutional affiliations.